

# Modelling of Cancer Stem Cell Driven Solid Tumors

Thomas Hillen and Alexandra Shyntar

**Abstract** Cancer stem cells (CSCs) are pluripotent cancer cells, which are less sensitive to treatments, and which can generate new tumors once transplanted into a healthy tissue environment. They have been identified in many cancers and they are the driving force of cancer growth and metastasis. Mathematical modelling of CSCs has contributed to our increased understanding of CSC interactions. Here we will consider CSC feedback mechanisms, treatments with radiation therapy, differentiation promoters, and dedifferentiation inhibitors. In addition, we will consider spatially explicit models. The dominating effect in these models is the *tumor growth paradox*. It says that a tumor under treatment might grow larger than a similar tumor without treatment. Using geometric singular perturbation methods, we prove mathematically that such a tumor growth paradox can arise. In the spatial context, it leads to a *tumor invasion paradox*, as we will explain. Many of the models presented here lead to interesting mathematical questions and to the development of new mathematical techniques. We end our chapter with a collection of open problems, which we think, are amenable to further mathematical analysis.

## 1 Introduction

The term “cancer” is a notion for a large collection of diseases, which share certain common hallmarks of cancer [23, 24, 22]. Medical research in oncology over the last decades has revealed a plenitude of cancer types, cancer dynamics, and cancer treatments. Cancer is no longer seen as an isolated disease; it rather arises as a complex interaction of cells of different genotypes, phenotypes, epigenetics, in a biochemical network of chemokines, growth factors, and antigens, in interaction with immune response, microenvironment, and treatments [23, 24, 22].

Just over twenty years ago, Hanahan and Weinberg published their landmark paper *The Hallmarks of Cancer* [23] where they outlined 6 key differences (“hallmarks”) between cancer tissue and normal tissue. These original six hallmarks were updated eleven years later in a second paper - *Hallmarks of Cancer: The Next Generation* [24], followed in 2022 by a third paper – *Hallmarks of Cancer: New Dimensions* [22]. As things stand now, the hallmarks of cancer consist of eight hallmark capabilities: (H1) sustained proliferative signalling, (H2) evading growth suppressors, (H3) resisting cell death, (H4) replicative immortality, (H5) angiogenesis, (H6) invasion and metastasis, (H7) reprogrammed metabolism, (H8) avoidance of immune destruction, plus two enabling characteristics: (H9) genome instability, (H10) tumor promoting inflammation; along with four more emerging hallmarks and enabling characteristics: (H11) phenotypic plasticity, (H12)

---

University of Alberta, Edmonton, Canada, e-mail: thillen@ualberta.ca. shyntar@ualberta.ca

epigenetics, (H13) the microbiome, and (H14) cell senescence. Reading this list is overwhelming. It shows why it is so difficult to properly understand cancer and to efficiently treat it. Researchers with many different expertise are needed to gain a full picture of this disease, and mathematics is one important partner in this research.

## 1.1 Cancer Stem Cells

A major player in the growth and spread of cancer are cancer stem cells (CSCs). These are pluripotent cells that are able to generate a full tumor if transplanted into new, healthy, environment [49, 10, 14]. Although the classification of CSCs is not uniform among cancers, or among scientists, the common features of CSCs often include the ability to self-renew, having unlimited replicative potential, immortality, and having reduced sensitivity to treatments such as radiation and chemotherapy [14, 32, 55]. CSCs are involved in many of the hallmarks mentioned above. They provide sustained growth signals (H1), evade growth suppression (H2), resist cell death (H3), have replicative immortality (H4), are involved in metastasis formation (H6), and can become senescent (H14). They are likely involved in the other hallmarks too. Hence, a good understanding of CSCs and their role inside the tumor environment is essential. CSCs have been identified in most cancers [14], and their relevance in cancer progression has been understood. In fact, Dingli and Michor [13] entitled their 2006 paper with *Successful therapy must eradicate cancer stem cells*.

One method to help gain an understanding of complex processes is mathematical modelling. Since the early models for cancer stem cells [2, 13, 19, 58], mathematical modelling of cancer stem cells is at full swing [39, 62, 31, 6, 60, 26, 61, 20, 50, 59, 7, 4, 54, 46, 34, 57].

CSCs are similar to healthy stem cells, however, healthy stem cells, for example in the hematopoietic system, give rise to various cell lineages of progenitor cells, transient amplifying cells and differentiated cells. Such a distinction is less clear for CSCs, hence in our modelling we only distinguish between stem and non-stem cancer cells. As our focus here is on solid tumors, we denote non-stem cancer cells as tumor cells (TCs).

## 1.2 Outline

For this book chapter, we begin with a very basic cancer stem cell model, and progressively consider model extensions to include many of the effects mentioned above. Writing down the basic CSC model already leads to confusion, since there are several ways to formulate the equations. For example, some authors use a probability of CSC self renewal as a model parameter, while others use a fraction of CSC offspring. Further, some scientists consider asymmetric divisions, while others consider symmetric divisions only. In the end, all these formulations are mathematically equivalent, and we will illustrate this equivalence in Section 1.3.

Having established the equivalence of the different model formulations, we add the defining feature of a solid tumor in tissue, which is having limited access to space and nutrients. We express this by a competition function  $F$  (see Section 1.4). The competition function leads directly to one of the key properties of the CSC model, which is the *tumor growth paradox*. It shows that increased treatment can lead to a larger tumor. This is a surprising effect that is related to the self-renewal properties of CSCs. In Section 2, we recall the arguments of [26] and use geometric singular perturbation theory to mathematically understand this phenomenon.

The model in [26] shows that treatments and immune responses can lead to CSC enriched cancers. Hence, it is a natural question to see if differentiation of CSCs into TCs can be promoted. Or if dedifferentiation of TCs into CSCs plays a role. Section 3.2 considers treatment of cancer with differentiation promoters such as

TGF- $\beta$  or all-trans-retinoic (ATRA) therapy. We combine this treatment with radiation and compare various model outcomes. We find that this combination of treatments shows great improvements for head and neck cancer and for metastatic brain cancer, but not so much for breast cancer. These results were published in [4].

In Section 3.3, we turn the differentiation process around and consider dedifferentiation. Dedifferentiation describes the process where differentiated cells, TCs, revert back and show stem cell like behavior. This process has been identified in many cancers [9, 33, 35]. In Section 3.3, we review a model from [50], which was developed to include the dedifferentiation promoter survivin and a survivin inhibitor YM155. Based on mice experiments of [30], we parametrize the model and again show that a combination therapy is beneficial. We also consider feedback mechanisms as modelled by [52, 34, 69] in Section 3.4. In that case, we account for chemokines that are released from CSCs and from TCs feedback on the self-renewal probability of CSCs. We show that some of these feedbacks can lead to an Allee effect.

In Section 4, we consider spatial versions of the CSC model. The first such model is developed closely to the experimental observations and takes the form of a birth-jump process (17). We show some general results on existence, uniqueness and positivity from [7, 38, 16]. The integral terms of the birth-jump model can be expanded as second order derivatives, which then leads to a reaction-diffusion model for CSCs and TCs. For this reduced model, we explain the *tumor invasion paradox*, which was proven in [57]. It describes the effect that a tumor with an increased death rate of TC invades faster.

We finish with a conclusion section, where the significance of these results is discussed and interesting open questions are presented.

### 1.3 Various CSC Models

To model the reproduction of cancer stem cells (CSCs) and their differentiation into non-stem cell tumor cells (TCs), we can use various approaches. We can use the probability of symmetric cell division into two CSCs, or use the frequency of CSC offspring through division, or use transition rates for the various possible mitosis events. We show a schematic in Figure 1. The left image in Figure 1 shows the full pathway, where CSCs divide with a rate  $k > 0$  and then produce two CSC with probability  $\alpha_1$  (symmetric division), two TCs with probability  $\alpha_3$ , or one CSC and one TC with probability  $\alpha_2$  (asymmetric division). In the middle image of Figure 1, it is assumed that one offspring replaces the mother cell and the second offspring is either a CSC with probability  $\delta$  or a TC with probability  $1 - \delta$ . In the third image of Figure 1, we only consider symmetric divisions into two CSC with probability  $p$  and into two TC with probability  $1 - p$ . These various formulations of symmetric versus asymmetric cell division have led to some confusion in the literature. Here, we quickly show that these approaches are all mathematically equivalent where a simple redefinition of the parameters leads from one form to the other.

We begin with the complete model that is illustrated on the left of Figure 1. We denote the CSC population by  $u(t)$  and the TC population by  $v(t)$ , and we assume that  $k > 0$  is the (constant) mitosis rate. Upon mitosis, a CSC can divide symmetrically into two CSCs, asymmetrically into one CSC and one TC, or symmetrically into two TCs. Each of these transitions happen with a probability of  $\alpha_1$ ,  $\alpha_2$ , and  $\alpha_3$ , respectively. Note that  $\alpha_1 + \alpha_2 + \alpha_3 = 1$  and if we multiply such a fraction by  $k$ , then we obtain the effective rates for these transitions. For example  $k\alpha_2$  is the rate of asymmetric division. We ignore TC self-renewal for this argument.

The complete model can be expressed as

$$\begin{aligned}\dot{u} &= 2\alpha_1 ku - \alpha_1 ku - \alpha_3 ku, \\ \dot{v} &= \alpha_2 ku + 2\alpha_3 ku.\end{aligned}\tag{1}$$

Since  $\alpha_1 = 1 - \alpha_2 - \alpha_3$ , we can already eliminate one parameter:

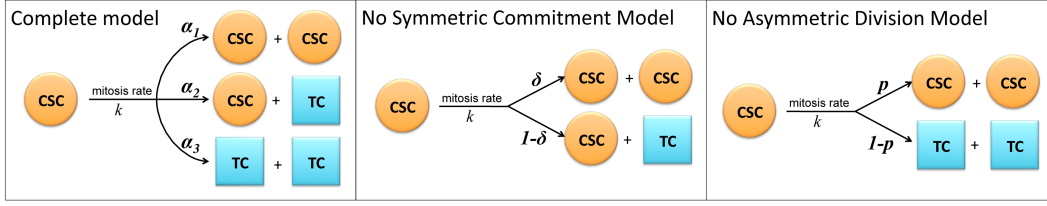


**Fig. 1** Schematics for the three ways a CSC model can be derived. In all model diagrams  $k$  is the mitosis rate. In the complete model,  $\alpha_1$ ,  $\alpha_2$ ,  $\alpha_3$  represent the probability of offspring comprised of two CSCs, probability of offspring comprised of one CSC and one TC, and probability of offspring comprised of two TCs, respectively. In the No Symmetric Commitment Model,  $\delta$  represents the fraction of CSC offspring. In the No Asymmetric Division Model  $p$  represents the probability of obtaining two CSCs as offspring.

$$\begin{aligned}\dot{u} &= (1 - \alpha_2 - 2\alpha_3)ku, \\ \dot{v} &= (\alpha_2 + 2\alpha_3)ku.\end{aligned}$$

Note that if  $\alpha_2 + 2\alpha_3 > 1$ , then the CSC population declines. Now, we set  $\delta := 1 - (\alpha_2 + 2\alpha_3)$  to obtain the model

$$\begin{aligned}\dot{u} &= \delta ku, \\ \dot{v} &= (1 - \delta)ku.\end{aligned}\tag{2}$$

These are the equations for the asymmetric division model that is shown in the middle of Figure 1. Note that in general  $\delta$  can be negative, which means that CSCs can decline. If  $\delta > 0$ , then  $\delta$  can be seen as the fraction (or probability) of offspring that are CSCs.

Finally, in the symmetric division model on the right of Figure 1, we denote by  $p$  the probability that division leads to two CSCs and by  $1 - p$  the probability that division leads to two TCs. The equations for this model are

$$\begin{aligned}\dot{u} &= 2pku - ku = (2p - 1)ku, \\ \dot{v} &= 2(1 - p)ku.\end{aligned}\tag{3}$$

If  $\delta = 2p - 1$ , then  $1 - \delta = 2(1 - p)$  and we obtain model (2) again. In reverse, if we define  $p = \frac{1}{2}(\delta + 1)$ , then model (2) leads to model (3). Hence (2) and (3) are fully equivalent.

Model (1) has two free parameters  $\alpha_2$  and  $\alpha_3$  and we cannot uniquely recover those from the knowledge of  $\delta$  or  $p$ . However, once  $\alpha_2$  and  $\alpha_3$  are given, the dynamics of (1) are fully described by any of the models (2) or (3). In the following sections, we will mostly use (2) and in cases where the probability  $p$  is important, we will also use model (3).

## 1.4 The Base Model

To obtain the base model for CSC driven solid tumors, we add three more effects into the model (2). First of all, we introduce a competition function  $F(n)$ , where  $n = u + v$  denotes the total cell population. As  $n$  increases, the availability of space and nutrients decreases until a certain carrying capacity  $K$  is reached. For  $n > K$  no reproduction is possible due to limited space and limited nutrients and the cells become quiescent. To be specific, we assume

(F)  $F(n)$  is Lipschitz continuous,  $F(0) = 1$ ,  $F$  is non-increasing, and  $F(n) = 0$  for all  $n \geq K$ .

Our standard example is  $F(n) = \max\{1 - n, 0\}$  and  $K = 1$ .

We also include TC self renewal with rate  $k_2$  and TC cell death with rate  $a$ . We do not (yet) include CSC death, since we assume that CSC are essentially immortal if unperturbed. Then our base model becomes

$$\begin{aligned}\dot{u} &= \delta k F(n) u \\ \dot{v} &= (1 - \delta) k F(n) u + k_2 F(n) v - av.\end{aligned}\tag{4}$$

## 2 The Tumor Growth Paradox

To explain how the tumor growth paradox arises from a mathematical point of view, we simplify a bit and assume that the growth rates for CSCs and TCs are the same and equal to one:  $k = k_2 = 1$ . The same arguments also hold for more general values, but the calculations would include additional growth rate ratios. With this, model (4) simplifies to a two-parameter model for the fraction of CSC offspring  $\delta$  and the TC death rate  $a$

$$\begin{aligned}\dot{u} &= \delta F(n) u, \\ \dot{v} &= (1 - \delta) F(n) u + F(n) v - av.\end{aligned}\tag{5}$$

**Definition 1** System (5) shows a tumor growth paradox, if there exist parameter values  $a_1 > a_2$  and an open time interval  $(t_1, t_2)$ , with  $0 < t_1 < t_2$  such that  $n^{a_1}(0) = n^{a_2}(0)$  and

$$n^{a_1}(t) > n^{a_2}(t), \quad \text{for all } t \in (t_1, t_2),$$

where  $n^{a_i} = u^{a_i} + v^{a_i}$  denotes the solution of (5) for death rate  $a = a_i$ ,  $i = 1, 2$ .

In other words, if we consider two versions of (5) with different death rates  $a_1 > a_2$  and the same initial condition, then there is a time where the tumor with the larger death rate of TCs becomes larger than the tumor with the lower death rate of TCs. A paradox.

In [26], we prove:

**Theorem 1** *Assume the conditions (F) and assume  $\delta > 0$  is small. Then (5) shows a tumor growth paradox.*

The proof uses a multiscale argument, which we like to present here in some detail. It gives a lot of insight into the dynamics of the model, and it prepares the arguments for later sections. The parameter  $\delta$  is assumed to be small enough such that the conditions of the Fenichel theorems of geometric singular perturbation theory are satisfied [25]. Please see [26] for those details on the scaling. Here, we simply assume  $\delta$  is small and as an example we use  $\delta = 0.01$  in our simulations. We use this  $\delta$  in an asymptotic expansion of model (5). If we set  $\delta = 0$  in (5), then we obtain the leading order term, also called the *fast system*:

$$\begin{aligned}\dot{u} &= 0 \\ \dot{v} &= F(n) u + F(n) v - av.\end{aligned}\tag{6}$$

We rescale time by setting  $\tau = \delta t$ , which describes a macroscopic time, also called the slow time scale. If we perform this transformation in (5) and then look at the leading order term, we obtain the *slow system*

$$\begin{aligned}\frac{d}{d\tau} U &= F(N) U \\ 0 &= F(N)(U + V) - aV.\end{aligned}\tag{7}$$

Here we use capital letters  $U, V, N = U + V$ , to distinguish the slow system (7) from the fast system (6). The second equation from (7) is an algebraic equation for  $U$  and  $V$ . In the  $(U, V)$  phase space it defines a manifold, called the *slow manifold*

$$M := \{(U, V) \in \mathbb{R}^2 : F(U + V)(U + V) = aV\}.$$

We plot this manifold for three different values of  $a = 0.1, 0.5, 1$  in Figure 2 (A). The first equation of (7) describes the dynamics on  $M$ . As  $F(N) > 0$  for  $N < 1$ , the dynamics on  $M$  is a continued growth until  $N = 1$ .

The fast system (6) describes the fast approach onto the manifold  $M$ . In our case  $u(t) = \text{constant}$  and the  $v$ -nullcline of the fast system is the slow manifold  $M$ . The Fenichel theory of geometric singular perturbation, which is nicely presented in [25], now ensures that the orbits of the full model (5) follow the fast system until they reach  $M$ , and then follow the slow system on  $M$ . In Figure 2 (B), we show three orbits of the model (5) for different values of  $a = 0.1, 0.5, 1$ , which all start at the same initial value  $(u(0), v(0)) = (0.01, 0.05)$ , and all end at time  $t = 1000$ . In all three cases we see a quick vertical growth until the corresponding slow manifold is reached. Then the orbits follow their corresponding  $M$ . Notice that the blue curve corresponds to the lowest death rate  $a = 0.1$ , while the red curve corresponds to the larger rate  $a = 1$ . The blue curve raises much higher in the  $v$ -component, while the red curve advances further in  $u$ -direction. To see the total population  $n = u + v$  at  $t = 1000$ , we include three helper lines for the levels of  $n = 0.8, 0.9$ , and  $1$ . Using this information, we see clearly that the red curve (large  $a$ ) has advanced further beyond the 0.9 level than the green curve (medium  $a$ ) and the blue curve (small  $a$ ), showing the tumor growth paradox in action. We also note that larger  $a$  selects for a CSC enriched tumor (larger  $u$ -values).

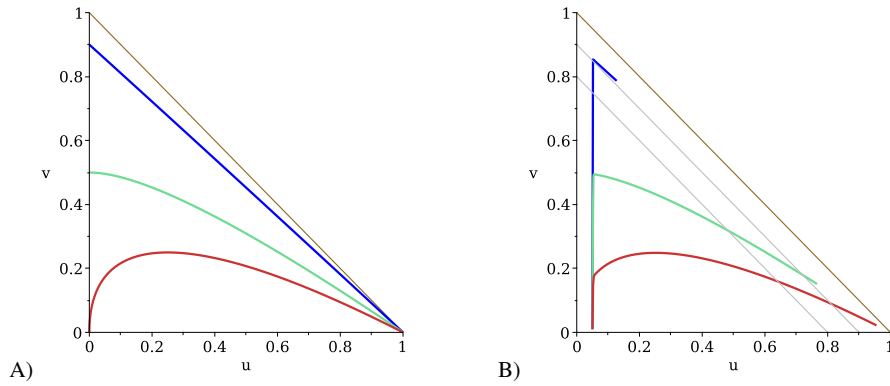


**Fig. 2** A) The slow manifolds  $M$  in the phase space for  $a = 0.1$  in blue,  $a = 0.5$  in green and  $a = 1$  in red. B) Three orbits with a common initial condition but with different  $a$  values illustrating the tumor growth paradox, blue:  $a = 0.1$ , green  $a = 0.5$ , red:  $a = 1$ . Gray lines denote the levels of  $u + v = 0.8, 0.9, 1.0$ .

### 3 Inclusion of Treatments and Feedbacks

To discuss the inclusion of treatments, we will present three scenarios. In the first case, we use a hypothetical treatment on-off situation, which enables us to explain the dynamics using the slow manifold technique from above. In that case, no attempt was made to fit to specific cancer data or cancer treatments. In Section 3.2 however, we review the results from [4] and parameterize the model for differentiation therapy of head and neck cancer, breast cancer, and metastatic brain cancer. We will see that combination of differentiation promoters and radiation treatment can have large beneficial effects for the patients. In Section 3.3, we consider a model given in [50], where we included an anti-survivin treatment for non small cell lung cancer (NSCLC). Survivin promotes TC dedifferentiation into CSCs, and a treatment with YM155 (*sepantronium bromide*) inhibits survivin, i.e. inhibiting dedifferentiation [30, 42]. A fit to mouse data of NSCLC shows a significant effect of YM155 treatment. In section 3.4 we include feedback mechanisms that arises through cytokines that are released from the growing tumor. We find growth inhibition and Allee effects related to those feedbacks.

### 3.1 General treatments

The slow manifold analysis is quite useful when including treatments. Mathematically, treatment changes the death rate  $a$  of TCs and it also affects CSCs. During treatment  $a$  is large and between treatments it is low. As we have seen, the slow manifold  $M$  depends on the value of  $a$ , where the manifolds with high values of  $a$  are lower in the phase plane than the manifolds for low  $a$  (see Figure 2). For a periodic treatment (such as fractionated radiation), we will have two manifolds to consider, a treatment-on manifold and a treatment-off manifold. The solution will jump between these. We illustrate this behavior in Figure 3 A), where we clearly see jumps between a higher arc (no treatment) and a lower arc (treatment).

The model that we use for Figure 3 is slightly modified, since if treatment is applied the CSCs will be affected, but to a lower degree. CSC have various resistance mechanism [14]. Hence, we consider

$$\begin{aligned}\dot{u} &= \delta F(n)u - a\kappa R(t)u \\ \dot{v} &= (1 - \delta)F(n)u + F(n)v - av - aR(t)v,\end{aligned}\quad (8)$$

where  $R(t)$  denotes the radiation treatment schedule. We multiply the radiation term by the natural death rate  $a$  such that the effect of  $R$  can be better compared to the death rate of  $v$ . As a simple example, we assume radiation is on for 200 time units and off for 200 time units. During treatments,  $R(t) = 10$  and in between treatments  $R(t) = 1$ . The simulations for initial condition  $(u_0, v_0) = (0.2, 0.2)$  are shown in Figure 3. Now the behavior depends on the size of the CSC resistance factor  $\kappa$ . If  $\kappa$  is small ( $\kappa = 0.001$  in Figure 3 (A)), then the disease progresses. If  $\kappa$  is intermediate ( $\kappa = 0.008$  in Figure 3 (B)) then we reach a periodic solution. This corresponds to cancer control but not to cancer removal. And finally, for large enough sensitivity of CSCs ( $\kappa = 0.02$  in Figure 3 (C)), we can observe treatment success.

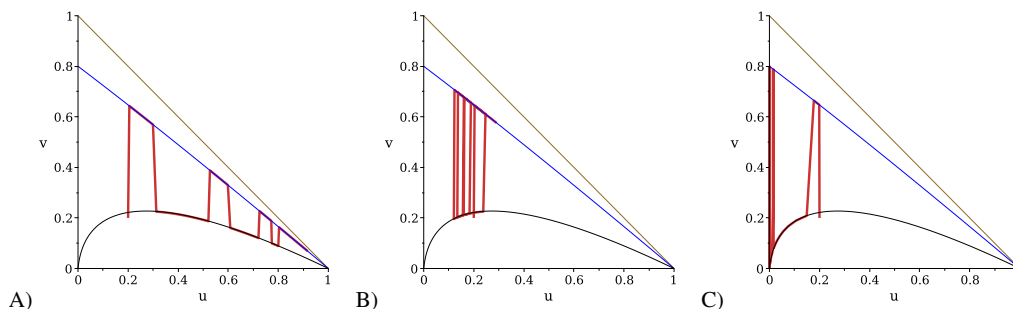


**Fig. 3** Typical treatment scenarios with initial condition  $(u_0, v_0) = (0.2, 0.2)$ . A) The CSCs are minimally affected and  $\kappa = 0.001$ . The disease progresses along the slow manifolds of on-treatment and off-treatment. B) Here  $\kappa = 0.008$  and CSCs are sensitive to the treatment. We obtain a trade off between tumor shrinkage during treatment and tumor regrowth in between treatments. If treatment was repeated indefinitely, we would end up in a periodic orbit. In C), we use  $\kappa = 0.02$ , which leads to full elimination of the cancer. The slow manifold for no-treatment is shown as a thin blue line and the on-treatment manifold is shown in black.

### 3.2 Differentiation Therapy

Since CSCs are less sensitive to treatments [32, 44, 14], it might be possible to use drugs that force CSCs to differentiate, thereby reducing the number of CSCs and increasing the sensitivity for treatments. As discussed in [36, 64, 40, 69], members of the TGF- $\beta$  family are known to increase differentiation. TGF- $\beta$

also affects other cancer characteristics such as immune evasion, but here we focus on the role on CSCs differentiation. In case of leukemia, a differentiation promoting therapy, called ARTA therapy, was discussed in [55], and in case of melanoma, interferon  $\beta$  and mezerein were considered as differentiation promoters [37].

Youssefpour et al. [69] developed a very detailed CSC model, which not only includes CSCs and TCs, but also transient amplifying cells, chemokine induced feedback mechanisms, spatial dependence and mechanical forces. They show that a differentiation promoter in combination with radiation treatment can have beneficial effects, allowing reduced radiation doses to be used to achieve treatment success. In [4], they use our simple model from above, to specifically consider parameter values for three cancers: head and neck, breast, and metastatic brain tumors.

To include a differentiation promoter, we follow the choice of [69] and modify the probability of symmetric CSC division as function of a differentiation promoter concentration  $C(t)$  as

$$p(t) = p_{\min} + (p_{\max} - p_{\min}) \frac{1}{1 + \psi C(t)}, \quad (9)$$

where  $p_{\max}$  is the self-renewal probability without any treatment and  $p_{\min}$  is the minimum self renewal probability at maximal treatment. The parameter  $\psi$  represents the sensitivity of the CSC to the chosen drug. Since the effect of the differentiation promoter affects the probability  $p$ , we use the model formulation (3) as our base model. We recall that the  $p$  relates to  $\delta$  as  $\delta = 2p - 1$ . In our simulations, we chose  $p_{\max} = 0.505$ , which corresponds to  $\delta = 0.01$ , as chosen before. We chose  $p_{\min} = 0.2$  as in [69], which gives a negative  $\delta = -0.6$ , i.e. CSC die out at large doses of  $C(t)$ .

To describe radiation damage, we use the standard linear-quadratic model (LQ-model). It describes the surviving fraction of cells that are exposed to a dose  $d$  as

$$S(d) = e^{-\alpha d - \beta d^2}. \quad (10)$$

The parameters  $\alpha$  and  $\beta$  denote the radio sensitivities of the tissue at hand. These values are well known for cancer and healthy tissues, and we will consider typical values for three cancer types: head and neck, metastatic brain cancer, and breast cancer (see Table 1). The  $\alpha$  term corresponds to a single hit action, i.e. DNA damage that results from direct interaction of radiation with DNA [17, 67]. The  $\beta$ -term represents double-hit action, where two non-lethal single hit events interact to form lethal damage. In our model, we assume that CSCs have an increased ability of damage repair, hence we chose  $\beta = 0$  for CSC.

There are (at least) two methods to include fractionated radiotherapy into an ODE model of cancer. One method is to stop the ODE model at the treatment time, and apply the surviving fraction (10) to the solution. The new values will then be used as new initial conditions to solve the ODE for the next non-treatment period. Alternatively, we can include the surviving fraction directly into the ODE formulation via the hazard function approach. As shown in detail in [21], the hazard function for fractionated treatment of dose  $d$  per fraction is given as  $h(t) = (\alpha + \beta d)\dot{D}$ , where  $\dot{D}$  is the dose rate during treatment (for example 2 Gy per hour). In our case we have two hazard functions, one for CSC and one for TC as

$$h_{\text{CSC}}(t) = \alpha \dot{D}, \quad h_{\text{TC}}(t) = (\alpha + \beta d)\dot{D}.$$

Hence our modified model for combination treatment with differentiation promoter and radiation treatment becomes

$$\begin{aligned} \dot{u} &= (2p(t) - 1)kF(n)u - h_{\text{CSC}}(t)u \\ \dot{v} &= 2(1 - p(t))kF(n)u + kF(n)v - av - h_{\text{TC}}(t)v, \end{aligned} \quad (11)$$

where we also include the growth rate  $k$ .

In [4], we present a full analysis of this model for different cancers and with different schedules for  $C(t)$ . For these cases, we also computed the tumor control probability and analysed how it depends on

the combination treatment. Here, we take a little simpler approach, which conveys the same message. We consider radiation treatment for the first week (5 treatment days), and vary the probability of CSC self renewal between its minimum  $p_{\min}$  and maximum  $p_{\max}$  values. The other model parameters are chosen from the literature shown in Table 1.

Parameter	Head and Neck	Brain	Breast
$\alpha/\beta$	10	12	2.88
$\alpha$ ( $\text{Gy}^{-1}$ )	0.35	0.3	0.08
$\beta$ ( $\text{Gy}^{-2}$ )	0.035	0.025	0.027
$d$ (Gy)	2.53	3.8	2.26
$k$ (1/h)	0.027	0.021	0.007

**Table 1** Model parameters. The parameters for head and neck cancer were taken from [18], the values for metastatic brain cancer from [70], and those for breast cancer from [48, 47].

Figure 4 shows the corresponding solutions of model (11). We show the CSC population in red and the TC population in blue. The case of maximal CSC self renewal  $p = p_{\max}$  as shown in bold lines while the minimal self renewal  $p = p_{\min}$  cases are shown as thin line. The value  $p = p_{\max}$  corresponds to the absence of differentiation promoter, while the case  $p = p_{\min}$  assumes maximal differentiation promoter effect. Figures 4 (A), (B), and (C) show the corresponding plots for head and neck cancer, metastatic brain cancer, and breast cancer, respectively.

We observe the largest effect of differentiation promoter for the head and neck case (A). The thin lines are clearly below the bold lines, and the tumor declines much quicker under differentiation treatment. In the case of metastatic brain cancer (B), we see that treatments with and without differentiation promoter are efficient, while for breast cancer both treatments are less efficient. In each case we get slight improvement by using a differentiation promoter. For a more detailed analysis of these cases see [4].

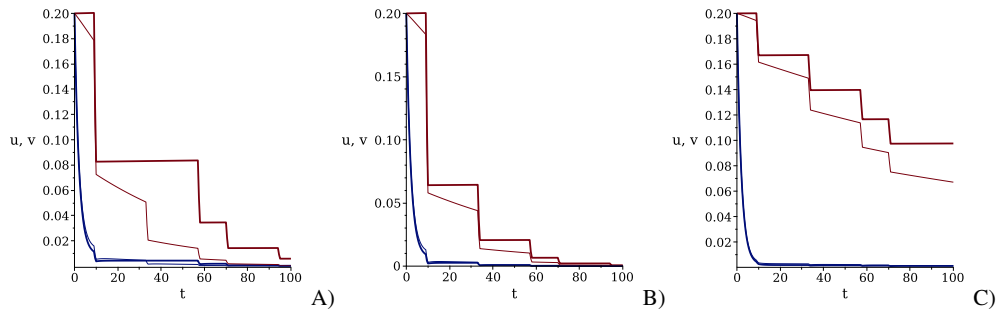


**Fig. 4** In each figure, CSCs are represented by the red curves and TCs are represented by the blue curves. Bold curves represent the absence of a differentiation promoter in treatment and the thin curves represent the presence of a differentiation promoter in treatment. The time is shown in hours (120 hrs = 5 days), and radiation treatment of  $2\text{Gy}$  is applied on each day at 9 AM for one hour. Figures A), B), C) represent the cases for head and neck cancer, metastatic brain cancer, and breast cancer, respectively. In A) the treatment with a differentiation promoter is significantly better at reducing the CSCs, whereas there is less difference between treatments in C), but the treatment with a differentiation promoter is still more effective.

### 3.3 Survivin and Dedifferentiation

Since the work of Takahashi [63], it is known that non-stem cancer cells can, potentially, reverse differentiation and express stem-cell like behavior. This process of *dedifferentiation* has been reported in many cancers [9, 33, 35]. As non stem tumor cells (TCs) are more sensitive to radiation, dedifferentiation can lead to radioresistance. Dahan [11] found that the inhibitor of apoptosis protein *survivin* supports dedifferentiation. Survivin has a low expression in healthy tissue [3], while it is over expressed in embryonic tissue and in cancer tissue. Furthermore, survivin expression increases upon radiation treatment, thereby reducing apoptosis and increasing radioresistance [11]. Nakahara [42] found that *sepratonium bromide* (YM155) reduces the expression of survivin, and can be used as survivin inhibitor in treatments. Iwasa [29] used these observations to design a detailed mouse model. They consider immuno suppressed mice that carry a human NSCLC and perform four types of experiments: (i) a control case of no treatment, (ii) a radiation treatment of 2 Gy per day for 5 days, (iii) a YM155 treatment, and (iv) a combination of radiation and YM155 treatments. In [50] a CSC-based mathematical model was developed to fit to the data of Iwasa [29]. The model fits the data very well and supports the conclusion that survivin plays an important role in cancer radio resistance.

Here, we review the model of [50] and explain the effects of survivin inhibition on a simplified treatment model. The above base model (4) is extended by a third compartment  $s(t)$  for the survivin concentration, plus dynamics that result from survivin:

$$\begin{aligned}\dot{u} &= \delta k F(n)u + \mu(s)v - \tau_s(s)u, \\ \dot{v} &= (1 - \delta)k F(n)u + k_2 F(n)v - \mu(s)v - \tau_d(s)v, \\ \dot{s} &= \omega_d \tau_d(s)v + \omega_s \tau_s(s)u - \sigma s,\end{aligned}\tag{12}$$

where  $\mu(s)$  describes the survivin-induced dedifferentiation and  $\tau_d(s)$ ,  $\tau_s(s)$  are the survivin dependent death rates of CSCs and TCs, respectively. The parameters  $k$  and  $k_2$  denote the base rates of mitosis for CSCs and TCs, respectively. The factors  $\omega_d$ ,  $\omega_s$  denote the survivin production rates based on cell apoptosis events and the rate  $\sigma$  denotes the rate of survivin clearance. We chose to describe the availability of space with the nonlinear function

$$F(n) = \max\{1 - n^4, 0\}$$

since cells are deformable and they can squeeze into open spaces [43]. The functional forms of the survivin dependent rates were chosen according to [69, 50]. The survivin dependent death rates are decreasing functions of  $s$ , since survivin is an anti-apoptotic protein:

$$\tau_s(s) = \frac{\tau_{d\max}}{1 + \theta_s s}, \quad \tau_d(s) = \frac{\tau_{s\max}}{1 + \theta_d s}.\tag{13}$$

The survivin-induced dedifferentiation rate  $\mu(s)$  is chosen to be a sigmoid function

$$\mu(s) = \frac{\mu_{\max}}{1 + \left(\frac{\mu_{\max} - \mu_{\min}}{\mu_{\min}}\right)^{1 - \frac{s}{s_2}}}.\tag{14}$$

And finally, radiation was modelled by the linear quadratic model as done before in (10). In [50], a detailed model fitting of the model (12,13,14) to the experimental data of Iwasa [29] was performed. In Table 2, we list the parameters that best fit those data.

In Figure 5, we show some model simulations with the parameter values from Table 2. In Figure 5 A), the dashed lines show the tumor evolution as a function of time for the untreated (control) case. The dark blue (dashed) line shows the CSC compartment, while the light blue line shows the TCs. Survivin concentration is shown in pink. We clearly see the growth of a stem-cell driven tumor. The thin solid lines show the case where survivin production is inhibited (for example by YM155). In that case, the tumor is TC dominated

**Table 2** Parameter values used for the survivin model (12).

Parameter	meaning	value from [50]
<b>initial conditions</b>		
$u(0)$	initial CSC density	0.0025
$v(0)$	initial TC density	0.05
$s(0)$	initial <i>survivin</i> concentration	0.0004
<b>model parameters</b>		
$\delta$	fraction of CSC after mitosis of CSC	0.01
$k(\text{time}^{-1})$	CSC mitosis rate	0.0659
$k_2(\text{time}^{-1})$	TC mitosis rate	0.6256
$\tau_{\text{max}}(\text{time}^{-1})$	max CSC death rate	0.002
$\tau_{\text{dmax}}(\text{time}^{-1})$	max TC death rate	0.5
$\mu_{\text{max}}(\text{time}^{-1})$	max rate of dedifferentiation	1.0997
$\omega_s(\text{time}^{-1})$	CSC <i>survivin</i> release	77
$\omega_d(\text{time}^{-1})$	max TC <i>survivin</i> release	55
$\sigma(\text{time}^{-1})$	<i>survivin</i> decay rate	0.475
$\theta_s(\text{concentration}^{-1})$	CSC <i>survivin</i> sensitivity	250
$\theta_d(\text{concentration}^{-1})$	TC <i>survivin</i> sensitivity	125
$\mu_{\text{min}}(\text{time}^{-1})$	min rate of dedifferentiation	0.000001
$s_2(\text{concentration})$	$\frac{\mu_{\text{max}}}{2}$ <i>survivin</i> concentration	0.1187
<b>radiation parameters</b>		
$\alpha/\beta$ (Gy)	NSCLC LQ ratio	10
$\alpha_s$ (Gy <sup>-1</sup> )	CSC DNA damage single tract	0.02465
$\alpha_d$ (Gy <sup>-1</sup> )	TC DNA damage single tract	0.2465
$\beta_s$ (Gy <sup>-2</sup> )	CSC DNA damage double tract	0.002465
$\beta_d$ (Gy <sup>-2</sup> )	TC DNA damage double tract	0.02465

(golden curve) with a very small CSC compartment (black line) and zero *survivin* (purple). The tumor grows slower and the composition is very different. We expect that the increased TC fraction in the case of inhibited *survivin* will make this tumor much more radiosensitive.

To show this effect, we apply radiation of 5 Gy on day 3 and day 7 in Figure 5 B). Here, the dashed lines show the growth of the total tumor  $u(t) + v(t)$  as functions of time without radiation. The base case is in black and the *survivin*-inhibited case in red. The corresponding thin lines include radiation, which can clearly be seen by the jumps on days 3 and 7. Radiation in the base case (thin black line) has a positive effect on delaying the cancer growth for a few days. But it does not control the cancer. However, radiation applied to the *survivin*-inhibited case (thin red line), has a drastic effect. On day 7 the cancer gets close to zero, which can be sufficient for treatment success if random perturbations are included. Even if it is not eradicated, the growth has been significantly delayed through the combination therapy of *survivin* inhibition and radiation treatment.

These simulations, and the more detailed analysis in [50], confirm Iwasa's [29] conclusion that *survivin* inhibition might be a suitable strategy to reduce radio-resistance in cancer cells.

### 3.4 Inclusion of Feedback Mechanisms

Rodriguez-Berens et al. [52, 68] used a simple variation of (4) to study feedback mechanisms that control CSC self renewal. In the experiments of Lander and others [36, 68], two effects were identified. The first effect is that a growing TC compartment down-regulates the proliferation rate  $k$ . Secondly, the growing TC compartment reduces the probability of CSC self renewal  $p$ . Hence in [52], they assume that both  $k(v)$  and  $p(v)$  depend on the TC compartment as strictly decreasing functions, which converge to 0 as  $v \rightarrow \infty$ . Their

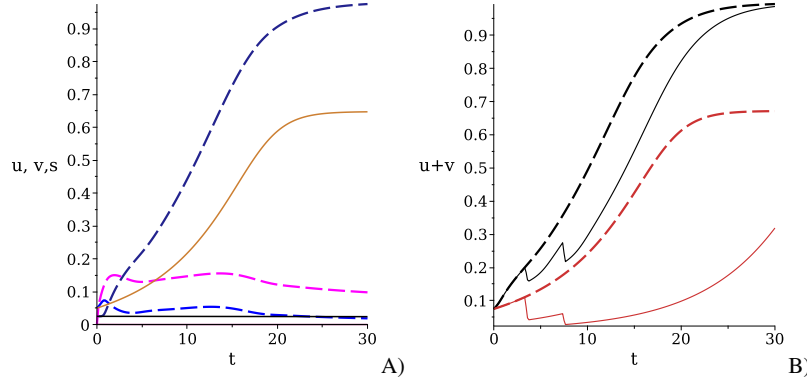


**Fig. 5** A) dashed curves show the solutions of the survivin model (12) without treatment, CSCs dark blue, TCs blue, survivin pink; the solid lines are the model with survivin inhibition, CSCs in black, TCs in gold and survivin in purple. B) Total cancer population  $u(t) + v(t)$  as function of time for the four cases: survivin + no treatment in dashed black, survivin + treatment in solid black, no survivin + no treatment in dashed red and no survivin + treatment in solid red.

model reads

$$\begin{aligned}\dot{u} &= (2p(v) - 1)k(v)u \\ \dot{v} &= 2(1 - p(v))k(v)v - av.\end{aligned}\quad (15)$$

Compared to (4), this model has no TC self renewal (i.e.  $k_2 = 0$ ) and also no volume mechanism (i.e.  $F(n) \equiv 1$ ). The authors chose  $p(0) > 0.5$  as otherwise the cancer would not grow in the first place. Using the above model (15), they find in [52] that growth control depends significantly on the self renewal probability  $p(v)$  and feedback on  $p$  is essential. Roughly speaking, we need to achieve  $p(v) < 0.5$  for large values of  $v$  such that CSCs can decay. Feedback in the division rate  $k(v)$  will only change the speed of growth, but will not control tumor growth [52].

In the context of colorectal cancers, it has been found that healthy stem cells and also cancer stem cells release the molecule Wnt as a self renewal promoter [1], thereby creating a positive feedback between CSC growth and CSC self renewal. Hence in Konstorum et al. [34], they included such a positive feedback into the CSC model. A self renewal promoter  $w(t)$  is included, and, as before, TGF- $\beta$  is modelled as differentiation promoter  $C(t)$ . The CSC model then becomes

$$\begin{aligned}\dot{u} &= (2p(C, w) - 1)ku \\ \dot{v} &= 2(1 - p(C, w))ku - av \\ \dot{C} &= \nu v - \mu C \\ \dot{w} &= w \left( \frac{\beta u w}{1 + \lambda w} - 1 \right),\end{aligned}\quad (16)$$

where the probability of CSC self renewal is increasing in  $w$  and decreasing in  $C$  with a functional form as in (9)

$$p(C, w) = p_{\min} + (p_{\max} - p_{\min}) \frac{\xi w}{1 + \xi w} \frac{1}{1 + \psi C},$$

and  $p_{\min}, p_{\max}, \xi, \psi > 0$  are constants. The differentiation promoter  $C$  is produced by the TC at rate  $\nu > 0$  and decays at rate  $\mu > 0$ . The growth activator  $w$  shows saturated growth with a finite carrying capacity and the coefficients  $\beta$  and  $\lambda$  are constant. In [34], the model (16) is simplified by assuming that  $C$  and  $v$  are in quasi steady state. In our words this means that we look at the dynamics of (16) on the slow manifold. For this reduced system, the existence of an Allee effect is shown in [34]. If the CSC and self promoter

$w$  are too small, then the CSC population dies off. The tumor can only grow if there is a sufficiently large CSC and  $w$  compartment. This observation has consequences for treatment since cancer does not need to be fully extinct via treatment. Rather, it is sufficient to reduce its size below an Allee threshold, such that the tumor can no longer self sustain and dies out. It is really interesting to see that such a positive feedback loop between CSC and  $w$  can produce an Allee effect. In the above two models (15) and (16), we did not include TC self renewal (i.e.  $k_2 = 0$ ) and neither the volume filling constraints  $F(n)$ . It is an interesting question to include TC self renewal  $k_2 \neq 0$  and volume filling terms  $F(n)$  in these models to see how the results change with the inclusion of these effects.

## 4 Spatially Explicit Models for CSCs

As we now understand the cancer stem cell model and its modifications very well, it is time to put it into the spatial context. We could simply, as many authors do, add diffusion terms to the equations of (4). This however, appears too naive for our purpose. Rather, we take guidance from the work of Enderling et al. [15, 65], where a spatial cancer stem cell model was developed as an individual based cellular automaton. They consider a square grid where each grid cell can be either occupied by a CSC or a TC, or be empty. Cells can divide if nearby empty cells are available. Otherwise, they stay quiescent or die. In addition, cells are able to randomly move to nearby grid cells, if space is available. The CSCs have unlimited replicative potential, while the TCs can only divide a limited amount of time. In simulations, it is seen that CSCs surround themselves with TCs, which in turn occupy space and inhibit further CSC divisions. CSCs become trapped and tumor growth stops. Once TCs are removed, say via treatment, space for CSC division and movement becomes available which results in more CSCs, eventually leading to a larger tumor. This effect is known as the *tumor growth paradox*. In [15], the ability of cells to move randomly seemed important, as otherwise the tumor growth paradox would not arise.

### 4.1 Birth-Jump Models

Here we take the rules of Enderling's cellular automaton model [15] and formulate them as a spatial continuous model, using the framework of birth-jump models [27]. A birth-jump process is a process where population growth and spread are not decoupled but rather interdependent. In our context, we assume that upon division one daughter cell replaces the mother, while the other daughter cell is redistributed locally to some empty space. Mathematically, we introduce a spatial relocation kernel  $K(x, y)$  and as before a function for the volume effect  $F(n)$ . We denote the spacial domain by  $\Omega$  and for  $K, F, \Omega$  we assume:

$$(A.1) \quad K \geq 0, K \in C(\bar{\Omega}, \bar{\Omega}), K \in L^2(\Omega \times \Omega), \int_{\Omega} K(x, y) dx = 1, \int_{\Omega} K(x, y) dy \leq 1.$$

$$(A.2) \quad F : \mathbb{R}^+ \rightarrow [0, 1], F(0) = 1, F(n) = 0 \quad \text{for } n \geq 1$$

$F$  is non-increasing and Lipschitz continuous.

$$(A.3) \quad \Omega \subset \mathbb{R}^n \text{ is either a smooth bounded domain, or it is } \Omega = \mathbb{R}^n.$$

Then the spatially dependent cancer stem cell birth-jump model, introduced in [26], reads

$$u_t(x, t) = d_u \Delta u(x, t) + \delta k \int_{\Omega} K(x, y) F(n(x, t)) u(y, t) dy \quad (17)$$

$$v_t(x, t) = d_v \Delta v(x, t) + (1 - \delta) k \int_{\Omega} K(x, y) F(n(x, t)) u(y, t) dy + k_2 \int_{\Omega} K(x, y) F(n(x, t)) v(y, t) dy - av,$$

where again  $n(x, t) = u(x, t) + v(x, t)$  and  $d_u, d_v$  are diffusion coefficients. The above system needs to be equipped with appropriate boundary conditions, for example with the no-flux boundary conditions

$$\frac{\partial u}{\partial n} = \frac{\partial v}{\partial n} = 0, \quad \text{where } n \text{ denotes an outer normal on } \partial\Omega. \quad (18)$$

Maddalena et al. [38] provided a full solution theory for (17,18). The diffusion terms are the leading order differential operators. As they define strongly continuous semigroups of  $L^2$  and  $H^1$  spaces, we can consider the integral terms as compact perturbations. Then perturbed semigroup theory can be applied [45] to obtain unique local solutions. Furthermore, Maddalena et al. [38] show the following

**Theorem 2** *Assume  $n \leq 3$  and  $u_0, v_0 \in H^2(\Omega)$ . Then there exists a unique global solution of (17) with  $u(\cdot, t), v(\cdot, t) \in H^2(\Omega)$  and*

$$u(x, t) \geq 0, v(x, t) \geq 0, 0 \leq u(x, t) + v(x, t) \leq 1, \quad \text{for all } (x, t).$$

Moreover, Maddalena et al. [38] show with an energy principle, that all stationary states are spatially homogeneous. Hence, the model (17) excludes formation of small and stationary tumor masses. This is a serious short coming, since not all tumors continue to grow. The reason is the included diffusion terms, which always allow CSC and TC to escape and invade further.

In Borsi et al. [8] they consider the above model (17) without diffusion terms, i.e.  $d_u = d_v = 0$ . The leading order terms are now the non-linear integral operators and a semigroup method is not applicable. Instead, the authors use a fixed point argument. They assume for the initial conditions  $u_0(x), v_0(x)$  that

$$(B) \quad u_0, v_0 \in C(\bar{\Omega}), u_0 \geq 0, v_0 \geq 0, 0 \leq u_0 + v_0 \leq 1.$$

Using a-priori estimates and a fixed point argument, it was shown in [8]:

**Theorem 3** *Assume (A), (B) and  $d_u = d_v = 0$ . Then (17) has a unique global solution*

$$u, v \in C(\bar{\Omega} \times [0, \infty)),$$

with

$$u(x, t) \geq 0, v(x, t) \geq 0, 0 \leq u(x, t) + v(x, t) \leq 1, \quad \text{for all } (x, t).$$

Also, in Borsi et al. [8] numerical simulations were performed which again confirm the tumor growth paradox. We expect that the model (17) without diffusion would support finite size stationary tumors, but to prove this mathematically is an open question.

## 4.2 Reaction Diffusion Models

Spatial integral operators are in some sense close to differential operators. This can be seen for symmetric kernels  $K(|x - y|)$ , which have small variance and even smaller higher moments. We can expand the integral operator as

$$\begin{aligned} & \int_{\Omega} K(|x-y|)F(n(x,t))u(y,t)dy \\ & \approx F(n(x,t)) \left[ Au(x,t) + B_{ij}(x)\partial_i\partial_j u(x,t) + C_{ijkl}(x)\partial_i\partial_j\partial_k\partial_l u(x,t) + \text{h.o.t.} \right] \end{aligned} \quad (19)$$

where the partial symbols  $\partial_j$  stand for the partial spatial derivatives in direction  $x_j$ . The coefficients  $A, B, C$  denote the first even moments of  $K$ , where  $A$  is a scalar,  $B$  a 2-tensor and  $C$  a 4-tensor:

$$\begin{aligned} A &:= \int_{\Omega} K(|y|)dy, & B_{ij}(x) &= \frac{1}{2} \int_{\Omega} (x-y)_i(x-y)_j K(|y|)dy \\ C_{ijkl}(x) &= \frac{1}{24} \int_{\Omega} (x-y)_i(x-y)_j(x-y)_k(x-y)_l K(|y|)dy \end{aligned}$$

where the indices denote vector components and we use summation convention for repeated indices. Note that our earlier assumption (A) implies that  $A = 1$ .

Fasano et al. [16] looked at this case in one dimension up to order two. In this case, the diffusion cancer stem cell model becomes

$$\begin{aligned} u_t &= d_u u_{xx} + \delta k F(n)(u + B u_{xx}) \\ v_t &= d_v v_{xx} + (1 - \delta)k F(n)(u + B u_{xx}) + k_2 F(n)(v + B v_{xx}) - av \end{aligned} \quad (20)$$

The authors in [16] note that this problem is not well defined as a biological model, since the  $B u_{xx}$ -term in the second equation could lead to negative solutions for  $v$ , which is biologically unrealistic. They argue, however, that such a case is artificial and not be relevant in applications. Nevertheless, they show for model (20):

**Theorem 4** *Let  $u_0, v_0 \in C^{2+\gamma}(\mathbb{R})$  such that*

$$u_0(x) \geq 0, v_0(x) \geq 0, 0 \leq u_0(x) + v_0(x) \leq 1 - M$$

*for some small  $M > 0$ . Then (20) has a unique local classical solution  $u(x,t), v(x,t)$  which satisfies  $u(x,t) + v(x,t) \leq 1$  for all times  $t < T^*$ .*

In [57], we go one step further and also assume that  $B$  is small such that the  $B$ -terms can be ignored. This means the model simplifies further and becomes

$$\begin{aligned} u_t &= d_u u_{xx} + \delta k F(n)u, \\ v_t &= d_v v_{xx} + (1 - \delta)k F(n)u + k_2 F(n)v - av. \end{aligned} \quad (21)$$

This model does preserve positivity. It is also the model we would have obtained if we simply added diffusion terms to (4). However, now we know how it was derived and what assumptions were used to get to this model. Existence and uniqueness for model (21) is now covered by standard arguments for parabolic equations. The diffusion terms define a semigroup, and the other terms are globally Lipschitz-continuous perturbations, implying global classical solutions of (21) for standard boundary conditions [45].

A further interesting open problem arises if fourth order terms from the above expansion (19) were included. The effect on spatial invasion and regularity of solutions has not been studied yet.

### 4.3 The Tumor Invasion Paradox

With the above model (21), we come back full circle to the tumor growth paradox. In the spatial context, the tumor growth paradox leads to an increased cancer invasion speed for increased TC death rates. We call this a *tumor invasion paradox*. We can prove the tumor invasion paradox for a special case of (17). We assume the base mitosis rates for CSC and TC are the same and equal to one  $k = k_2 = 1$ . We also assume that the diffusion coefficients for CSC and TC are the same, since these are cells of similar size, and that diffusion is slow such that  $d_u = d_v = \delta d$ , for an order one value  $d$ . The resulting system becomes

$$\begin{aligned} u_t &= \delta d u_{xx} + \delta F(n)u \\ v_t &= \delta d v_{xx} + (1 - \delta)F(n)u + F(n)v - av. \end{aligned} \quad (22)$$

As in Section 2, we consider  $\delta$  to be small and use perturbation arguments. To leading order ( $\delta \rightarrow 0$ ), we obtain the fast system

$$\begin{aligned} u_t &= 0 \\ v_t &= F(n)u + F(n)v - av, \end{aligned} \quad (23)$$

which, as before, describes fast convergence towards the slow manifold

$$M := \{(u, v) : av = F(u + v)(u + v)\}.$$

Rescaling time as  $\tau = \delta t$  gives us the slow system, which to leading order becomes

$$\begin{aligned} u_t &= du_{xx} + F(u + v)u \\ 0 &= F(u + v)u + F(u + v)v - av. \end{aligned} \quad (24)$$

The second equation ensures that the dynamics are on the slow manifold  $M$ , while the first equation of (24) describes the dynamics on  $M$ .

In [57], we analyse the properties of the slow manifold in detail. We show that on  $M$ ,  $v$  can be written as a graph on  $u$ , i.e.  $v = v_a(u)$ . We use an index  $a$  to indicate that this map depends on the death rate  $a$ . Using this representation, we can write the first equation of (24) as an equation for  $u$  alone as

$$u_\tau = du_{xx} + F(u + v_a(u))u. \quad (25)$$

In [57], we show that this equation (25) is a bistable equation of Fisher-KPP type and we can look for travelling wave solutions. Travelling wave solutions are solutions that retain their shape and either propagate to the left or right with a constant speed. For example, a travelling wave solution propagating to the right can be written as  $u(x, t) = \varphi(x - ct)$  where  $c$  is a constant that defines the speed of the wave and  $\varphi(z)$  with  $z = x - ct$  gives the wave profile [12]. Additionally,  $\varphi$  satisfies

$$\varphi(-\infty) = 1 \quad \text{and} \quad \varphi(\infty) = 0.$$

This means that on the left the population density has reached its maximum size of 1, but the population has not yet arrived to the space on the right [12]. Since we know that (25) is of Fisher-KPP type, we can directly apply the known results on travelling waves for Fisher-KPP equations [66, 12]. To formulate the result, we define invasion initial conditions.

**Definition 2** A *invasion initial condition* for  $u_0(x)$  is a non-increasing function  $u_0(x)$  that satisfies

$$\lim_{x \rightarrow -\infty} u_0(x) = 1, \quad u_0(x) = 0 \text{ for all } x \geq x^*, \quad \text{for some } x^* \in \mathbb{R}.$$

We show in [57]:

**Theorem 5** We assume the previous assumptions (A) and (B),  $a > 0$  and that  $F'(n) < 0$  for  $0 \leq n \leq 1$ . We consider invasion initial conditions for  $u_0(x)$  and denote the solution of (25) with  $u(\tau, x)$ .

1. If  $a \geq 1$  then  $u(\tau, x)$  converges to a travelling wave with minimum wave speed

$$c^* = 2\sqrt{d}.$$

2. If  $a < 1$  then  $u(\tau, x)$  converges to a travelling wave with minimum wave speed

$$c^* = 2\sqrt{da}.$$

The cases connect continuously for  $a \rightarrow 1$ .

We see that for large  $a$  ( $a > 1$ ) the wave speed is independent of its value. However, for small  $a$  we see an invasion paradox. Reducing the death rate  $a$  reduces the invasion speed, quite contrary to what is expected.

We simulate (25) by choosing  $F = 1 - n$  where  $n = u + v$ . We choose this simple function  $F$  for the ease of computation since in [57] it was shown that any  $F$  satisfying the assumptions in Theorem 5 the resulting numerical solutions are very similar. We set  $d = 1$  for simplicity and focus on studying the death rates  $a = 3, 1, 0.5, 0.1$  as these highlight the key dynamics of the solutions to (25). By using the *pdepe* solver in MATLAB, we numerically obtain the travelling wave solutions of (25) shown in Figure 6. In these simulations, the initial condition is a step function where  $u_0(x) = 1$  for  $x < x^*$  and  $u_0(x) = 0$ , otherwise. We set  $x^* = 20$  and stop the simulation at  $\tau = 80$  to illustrate the main behaviour of the solutions given our parameter choices.

In Figure 6, we can clearly see the invasion paradox. For  $a \geq 1$ , we see that there is not much difference in the travelling wave solutions or invasion speeds as Theorem 5 states. However, for  $a < 1$ , as  $a$  decreases the travelling wave solutions become slower, illustrating the invasion paradox.

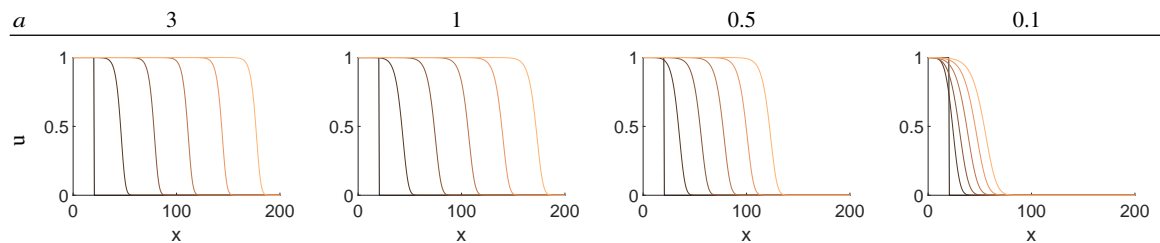


**Fig. 6** Travelling wave solutions at  $\tau = 0, 16, 32, 48, 64, 80$  of system (25). The value of  $a$  is given in column headers. The initial condition is a step function satisfying the invasion initial condition with  $x^* = 20$ . For death rates  $a = 3, 1$  no invasion paradox is present, whereas for  $a = 0.5, 0.1$  the invasion paradox can be observed where the solutions for  $a = 0.5$  invade faster into space than the solutions with  $a = 0.1$ .

In summary, the invasion paradox is an underlying property of (21). This shows that in addition to the tumor growth paradox, the invasion paradox may be at play. This means that cancer treatments may additionally increase tumor spread [57]. Fortunately, shorter treatments were shown to not significantly increase spread [57], but the invasion paradox becomes more significant in long term treatments.

## 5 Conclusions and Open Questions

The inclusion of CSC dynamics into solid tumor modelling adds another dimension to the discussion of tumor growth. On the one hand, CSCs are essential to keep a tumor growing, while on the other hand, CSCs can be blocked from space and nutrients making them quiescent. Once we wake them up, by liberating space or supplying nutrients, they divide again and possibly create a worse situation than before. Mathematically, this was expressed through the *tumor growth paradox* and the *tumor invasion paradox*. Through the spatial modelling, we observe a dichotomy between treatment-related tumor cell death and treatment induced spatial invasion. A fine balance needs to be achieved so that all CSCs are killed before the tumor can spread any further.

We included many cancer related effects into the modelling, such as treatments, combination therapies, feedback mechanisms, and spatial dependence. But this is just scratching the surface. Many interesting questions remain, and many of them are accessible to mathematical modelling. Here we like to summarize some of the questions that we find interesting for further study.

1. **Hallmarks:** We related the CSC modelling to the hallmarks (H1) sustained growth signals, (H2) evasion of growth suppression, (H3) resistance of cell death, (H4) replicative immortality, (H6) metastasis formation, and (H14) senescence. We expect that CSC play important roles in the other hallmarks as well, and a detailed modelling of those seems to be a natural place to continue. For example, the interaction of immune cells and CSCs is relatively poorly understood. There is indication [53] that CSCs evade immune destruction. This implies that an immune response would select for CSCs [26]. CSCs might also be able to re-educate immune cells to become pro-tumor immune cells [56, 51].
2. **Allee effect:** The Allee effect model (16) did not include the volume constraint  $F(n)$  and TC self reproduction. It would be interesting to extend the model (16) by including those terms and analyzing how the Allee threshold changes with those terms.
3. **Geometric singular perturbation theory for PDEs:** We saw that the slow manifold analysis is a quite powerful tool to understand the paradoxical behavior in tumor dynamics. For the ODE cases this is justified through the Fenichel theorems [25] for geometric singular perturbation theory. Unfortunately, such a theory is missing for the PDE models. Hence our scaling analysis in the PDE case is just a formal expansion without an abstract backbone behind it. Some early results for PDEs are available in the work of Bates et al. [5].
4. **Compact-support steady states for birth-jump models:** It would be important to understand possible steady states of the non-local spatial model (17) without diffusion, ( $d_u = d_v = 0$ ). Since the steady states represent solid tumors that stopped growing. We saw that if diffusion is added, steady states are constants [38]. However, without diffusion, we expect that non-constant steady states with compact support are possible. This will, of course, depend on the choice of the integral kernel  $K(x, y)$ .
5. **Tumor spheroids:** It would also be interesting to see the relative distribution of CSCs in a spatially extended tumor. There is extensive material available about CSC distributions in growing spheroids [28] and this material is just waiting for a mathematical analysis.
6. **Fourth order terms:** In the moment expansion of the integral term (19), Fasano et al. [16] stopped at the second order term (20). Many colleagues asked what would happen if the fourth order terms in (19) were included. In that case the model gets a Cahn-Hilliard [41] type structure, and phase separation phenomena might occur, where one phase describes tumor present and the other phase tumor absent. Interesting dynamics on the phase boundaries might occur.

## References

1. Stem cell signaling. an integral program for tissue renewal and regeneration: Wnt signaling and stem cell control. *Science* **346**(6205), 1248012 (2014)
2. Agur, Z., Daniel, Y., Ginosar, Y.: The universal properties of stem cells as pinpointed by a simple discrete model. *Journal of Mathematical Biology* **44**(1), 79–86 (2002)
3. Altieri, D.: Survivin, versatile modulation of cell division and apoptosis in cancer. *Oncogene* **22**, 8581–8589 (2003)
4. Bachman, J., Hillen, T.: Mathematical optimization of the combination of radiation and differentiation therapies of cancer. *Frontiers in Molecular and Cellular Oncology* (2012). URL doi: 10.3389/fonc.2013.00052. Free online, doi: 10.3389/fonc.2013.00052
5. Bates, P., Lu, K., Zeng, C.: Approximately invariant manifolds and global dynamics of spike states. *Inventiones Mathematicae* **174**(2), 355–433 (2008)
6. Beretta, E., Capasso, V., Morozova, N.: Mathematical modelling of cancer stem cells population behavior. *Math. Modelling of Natural Phenomena* **7**(1), 279–305 (2012)
7. Borsi, I., Fasano, A., Primicerio, M., Hillen, T.: Mathematical properties of a non-local integro-PDE model for cancer stem cells. *Math. Medicine and Biol.* **34**, 59–75 (2014)
8. Borsi, I., Fasano, A., Primicerio, M., Hillen, T.: Mathematical properties of a non-local integro-pde model for cancer stem cells. *Mathematical Medicine and Biology* **34**(1), 59–75 (2017)
9. Chaffer, C., Brueckmann, I., Scheel, C., et al.: Normal and neoplastic nonstem cells can spontaneously convert to a stem-like state. *Proceedings of The National Academy of Sciences* **108**(19), 7950–7955 (2011)
10. Clarke, M.F., Dick, J.E., Dirks, P.B., Eaves, C.J., Jamieson, C.H., Jones, D.L., Visvader, J., Weissman, I.L., Wahl, G.M.: Cancer stem cells—perspectives on current status and future directions: AACR workshop on cancer stem cells. *Cancer research* **66**(19), 9339–9344 (2006)
11. Dahan, P., Martinez Gala, J., Delmas, C., et al.: Ionizing radiations sustain glioblastoma cell dedifferentiation to a stem-like phenotype through survivin: Possible involvement in radioresistance. *Cell Death and Disease* **5**(11) (2014). Doi: 10.1038/cddis.2014.509
12. De Vries, G., Hillen, T., Lewis, M., Müller, J., Schönfisch, B.: A course in mathematical biology: quantitative modeling with mathematical and computational methods. SIAM (2006)
13. Dingli, D., Michor, F.: Successful therapy must eradicate cancer stem cells. *Stem Cells* **24**(12), 2603–2610 (2006)
14. Dittmar, T., Zänker, K.: *Role of Cancer Stem Cells in Cancer Biology and Therapy*. CRC Press, Boca Raton, FL, USA (2013)
15. Enderling, H., Anderson, A., M.A.J., C., Beheshti, A., Hlatky, L., Hahnfeldt, P.: Paradoxical dependencies of tumor dormancy and progression on basic cell kinetics. *Cancer Research* **69**(22), 8814–8821 (2009)
16. Fasano, A., Mancinia, A., Primicerio, M.: Tumours with cancer stem cells: A pde model. *Mathematical Biosciences* **272**, 76–80 (2016)
17. Fowler, J.: The linear quadratic formula and progress in fractionated radiotherapy. *Brit. J. of Radiology* **62**, 679–694 (1989)
18. Fowler, J.F.: 21 years of biologically effective dose. *British Journal of Radiology* **83**(991), 554–568 (2010)
19. Ganguli, R., Puri, I.: Mathematical model for the cancer stem cell hypothesis. *Cell Proliferation* **39**, 3–14 (2006)
20. Gao, X., McDonald, J., Hlatky, L., Enderling, H.: Acute and fractionated irradiation differentially modulate glioma stem cell division kinetics. *Cancer Research* **73**(5), 1481–90 (2013)
21. Gong, J., dos Santos, M.M., Finlay, C., Hillen, T.: Are more complicated tumor control probability models better? *Math. Med. Biol.* **30**(1), 1–19 (2011)
22. Hanahan, D.: Hallmarks of cancer: New dimensions. *Cancer Discovery* **12**, 31–46 (2022)
23. Hanahan, D., Weinberg, R.: The hallmarks of cancer. *Cell* **100**(1), 57–70 (2000)
24. Hanahan, D., Weinberg, R.: Hallmarks of cancer: The next generation. *Cell* **144**, 646–674 (2011)
25. Hek, G.: Geometric singular perturbation theory in biological practice. *J. Math. Biology* **60**(3), 347–386 (2010)
26. Hillen, T., Enderling, H., Hahnfeldt, P.: The tumor growth paradox and immune system-mediated selection for cancer stem cells. *Bulletin of Mathematical Biology* **75**(1), 161–184 (2013)
27. Hillen, T., Greese, B., Martin, J., de Vries, G.: Birth-jump processes. *J. Biol. Dynamics* **9**, 104–127 (2014). Doi: 10.1080/17513758.2014.950184
28. Ishiguro, T., Ohata, H., Sato, A., Yamawaki, K., Enomoto, T., Okamoto, K.: Tumor-derived spheroids: Relevance to cancer stem cells and clinical applications. *Cancer Science* **108**(3), 283–289 (2017)
29. Iwasa, T., Okamoto, I., Suzuki, M., et al.: Radiosensitizing effect of YM155, a novel small-molecule survivin suppressant, in non-small cell lung cancer cell lines. *Clinical Cancer Research* **14**(20), 6496–6504 (2008)
30. Iwasa, Y., Nowak, M., Michor, F.: Evolution of resistance during clonal expansion. *Genetics* **172**, 2557–2566 (2006)
31. Johnston, M., Maini, P., Chapman, S., Edwards, C., Bodmer, W.: On the proportion of cancer stem cells in a tumour. *J. Theor. Biol.* **266**, 708–711 (2010)

32. Kim, J., Tannock, I.: Repopulation of cancer cells during therapy: An important cause of treatment failure. *Nature Rev. Cancer* **5**, 516–525 (2005)
33. Klevebring, D., Rosin, G., Ma, R., et al.: Sequencing of breast cancer stem cell populations indicates a dynamic conversion between differentiation states in-vivo. *Breast Cancer Research* **16**(4) (2014). Doi: 10.1186/bcr3687
34. Konstorum, A., Lowengrub, J., Hillen, T.: Feedback regulation in a cancer cell model can cause an allee effect. *Bulletin Math. Biology* **78**(4), 754–785 (2016)
35. Lagadec, C., Vlashi, E., Donna, L.D., et al.: Radiation-induced reprogramming of breast cancer cells. *Stem Cells* **30**(5), 833–844 (2012)
36. Lander, A., Gokoffski, K., Wan, F., Nie, Q., Calof, A.: Cell lineages and the logic of proliferation control. *PLoS Biol.* **7**(1), e15 (2009)
37. Leszczyniecka, M., Roberts, T. P., D., Grant, S., Fisher, D.: Differentiation therapy of human cancer: basic science and clinical applications. *Pharmacology and Therapeutics* **90**, 105–156 (2001)
38. Maddalena, L.: Analysis of an integro-differential system modelling tumor growth. *Appl. Math. Comp.* **245**, 152–157 (2014)
39. Marciniak-Czochra, A., Stiehl, T., Ho, A., Jäger, W., Wagner, W.: Modeling of asymmetric cell division in hematopoietic stem cells—regulation of self-renewal is essential for efficient repopulation. *Stem cells and development* **18**(3), 377–386 (2009)
40. Meulmeester, E., Ten Dijke, P.: The dynamic roles of TGF-beta in cancer. *J. Pathology* **223**(2), 205–218 (2011)
41. Miranville, A.: *The Cahn–Hilliard Equation: Recent Advances and Applications*. SIAM Philadelphia (2019)
42. Nakahara, T., Kita, A., Yamanaka, K., et al.: YM155, a novel small-molecule survivin suppressant, induces regression of established human hormone-refractory prostate tumor xenografts. *Cancer Research* **67**(17), 8014–8021 (2007)
43. Painter, K., Hillen, T.: Volume-filling and quorum sensing in models for chemosensitive movement. *Canadian Applied Mathematics Quarterly* **10**(4), 501–543 (2002)
44. Pajonk, E., Vlashi, E., McBride, W.: Radiation resistance of cancer stem cells: The 4 R's of radiobiology revisited. *Stem Cells* **24**(4), 639–648 (2010)
45. Pazy, A.: *Semigroups of Linear Operators and Applications to Partial Differential Equations*. Springer, New York (1983)
46. Poleszczuk, J., Hahnfeldt, P., Enderling, H.: Evolution and phenotype selection of cancer stem cells. *PLoS Comput. Biol.* **11**(3), e1004025 (2015)
47. Qi, X.S., White, J., Li, X.A.: Is  $\alpha/\beta$  for breast cancer really low? *Radiotherapy and Oncology* **100**(2), 282–288 (2011)
48. Rew, D.A., Campbell, I.D., Taylor, I., Wilson, G.D.: Proliferation indices of invasive breast carcinomas after in vivo 5-bromo-2'-deoxyuridine labelling: A flow cytometric study of 75 tumours. *British Journal of Surgery* **79**(4), 335–339 (1992)
49. Reya, R., Morrison, S., Clarke, M., Weissman, I.: Stem cells, cancer, and cancer stem cells. *Nature* **414**(6859), 105–111 (2001)
50. Rhodes, A., Hillen, T.: Mathematical modeling of the role of survivin on dedifferentiation and radioresistance in cancer. *Bulletin Math. Biol.* **78**(6), 1162–1188 (2016)
51. Rhodes, A., Hillen, T.: A mathematical model of the immune-mediated theory of metastasis. *Journal of Theoretical Biology* (2019). Submitted. Pre-print available at bioRxiv, DOI: 10.1101/565531
52. Rodriguez-Berens, I., Komarova, N., Wodarz, D.: Evolutionary dynamics of feedback escape and the development of stem-cell driven cancers. *Proceedings of the Royal Acad. Sci.* **108**(47), 18983–18911 (2011)
53. Schatton, T., Frank, M.: Antitumor immunity and cancer stem cells. *Ann. NY Acad. Sci.* **1176**, 154–169 (2009)
54. Scott, J., Hjelmeland, A., Chinnaiyan, P., Anderson, A., Basanta, D.: Microenvironmental variables must influence intrinsic phenotypic parameters of cancer stem cells to affect tumorigenicity. *PLoS Comput. Biol.* **10**(1), e1003433 (2014)
55. Sell, S.: Stem cell origin of cancer and differentiation therapy. *Critical Reviews in Oncol.* **51**, 1–28 (2004)
56. Shahriyari, L.: A new hypothesis: some metastases are the result of inflammatory processes by adapted cells, especially adapted immune cells at sites of inflammation. *F1000 Research* **5**(175) (2016). Doi:10.12388/f1000research.8055.1
57. Shyntar, A., Patel, A., Rhodes, M., Enderling, H., Hillen, T.: The tumor invasion paradox in cancer stem cell driven tumors. *Bulletin of Math. Biol.* **84**(139) (2022)
58. Sole, R., Rodriguez-Caso, C., Diesboeck, T., Saldance, J.: Cancer stem cells as the engine of unstable tumor progression. *J. Theor. Biol.* **253**, 629–637 (2008)
59. Sottoriva, A., Verhoeff, J., Borovski, T., McWeeney, S., Naurnov, L., Medema, J., Slood, P., Vermuelen, L.: Cancer stem cell tumor model reveals invasive morphology and increased phenotypical heterogeneity. *Cancer Res.* **70**(1), 46–56 (2010)
60. Stiehl, T., Marciniak-Czochra, A.: Mathematical modeling of leukemogenesis and cancer stem cell dynamics. *Math. Modelling of Natural Phenomena* **7**, 166–202 (2012)
61. Sun, Z., Komarova, N.: Stochastic control of proliferation and differentiation in stem cell dynamics. *Math. Biosci.* **240**, 231–240 (2012)
62. Swierniak, A., Kimmel, M., Smieja, J.: Mathematical modelling as a tool for planning anticancer therapy. *Europ. J. Pharmacology* **625**, 108–121 (2009)
63. Takahashi, K., Yamanaka, S.: Induction of pluripotent stem cells from mouse embryonic and adult fibroblast cultures by defined factors. *Cell* **126**(4), 663–676 (2006)

64. Watabe, T., Miyazono, J.: Roles of TGF-beta family signaling in stem cell renewal and differentiation. *Cell Res.* **19**(1), 103–115 (2009)
65. Weekes, S., Barker, B., Bober, S., Cisneros, K., Cline, J., Thompson, A., Hlatky, L., Hahnfeldt, P., Enderling, H.: A multicompartiment mathematical model of cancer stem cell-driven tumor growth dynamics. *Bull. Math. Biol.* (2014). To appear
66. Weinberger, H., Lewis, M., Li, B.: Analysis of linear determinacy for spread in cooperative models. *J. Math. Biol.* **45**, 183–218 (2002)
67. Wheldon, T.: *Mathematical Models in Cancer Research*. Adam Hilger (1988)
68. Wodarz, D., Komarova, N.: *Dynamics of Cancer, Mathematical Foundations of Oncology*. World Scientific, Singapore (2014)
69. Youssefpour, H., Li, X., Lander, A., Lowengrub, J.: Multispecies model of cell lineages and feedback control in solid tumors. *Journal of Theoretical Biology* **304**(0), 39–59 (2012)
70. Yuan, J., Wang, J.Z., Lo, S., Grecula, J.C., Ammirati, M., Montebello, J.F., Zhang, H., Gupta, N., Yuh, W.T.C., Mayr, N.A.: Hypofractionation regimens for stereotactic radiotherapy for large brain tumors. *International Journal of Radiation Oncology Biology Physics* **72**(2), 390–397 (2008)